4-27-2010

# Simulation of Nanowire Tunneling Transistors: From the Wentzel-Kramers-Brillouin Approximation to Full-Band Phonon-Assisted Tunneling

Mathieu Luisier
*Network for Computational Nanotechnology and Birck Nanotechnology Center*

Gerhard Klimeck
*Network for Computational Nanotechnology, Purdue University*, gekco@purdue.edu

# Simulation of nanowire tunneling transistors: From the Wentzel–Kramers–Brillouin approximation to full-band phonon-assisted tunneling

Mathieu Luisier[a] and Gerhard Klimeck
*Network for Computational Nanotechnology and Birck Nanotechnology Center, Purdue University, 207 South Martin Jischke Drive, Indiana 47907, USA*

(Received 21 November 2009; accepted 12 March 2010; published online 27 April 2010)

Nanowire band-to-band tunneling field-effect transistors (TFETs) are simulated using the Wentzel–Kramers–Brillouin (WKB) approximation and an atomistic, full-band quantum transport solver including direct and phonon-assisted tunneling (PAT). It is found that the WKB approximation properly works if one single imaginary path connecting the valence band (VB) and the conduction band (CB) dominates the tunneling process as in direct band gap semiconductors. However, PAT is essential in Si and Ge nanowire TFETs where multiple, tightly-coupled, imaginary paths exist between the VB and the CB. © *2010 American Institute of Physics*. [doi:10.1063/1.3386521]

## I. INTRODUCTION

Based on the cold injection of electrons from the valence band (VB) of a source contact into the conduction band (CB) of a drain contact, tunneling field-effect transistors (TFETs) are expected to help reduce the power consumption of integrated circuits by exhibiting room temperature subthreshold swings below 60 mV/dec. This 60 mV/dec turn-off characteristics is the intrinsic limit of conventional metal-oxide-semiconductor field-effect transistors (MOSFETs).[1,2] TFETs are very sensitive to the CB and VB profiles in the channel, requiring an excellent control of the electrostatic potential under the gate contact.[3] Hence, nanowire structures, due to their one-dimensional (1D) transport properties and their operation close to the quantum capacitance limit[4] are promising candidates as high performance TFETs.

A spatially thin and energetically low tunneling barrier is essential to obtain large drive currents in TFETs. It can be realized with low band gap materials such as InAs or with properly designed heterostructures such as Si–Ge where the band gap discontinuity between these two materials leads to an effective tunneling gap of only 0.3 eV.[5–7] To accelerate the development in TFETs, it is crucial that the selection of the material system and the design of the transistor structure are critically analyzed with computer aided design tools before experiments are extensively conducted. The Wentzel–Kramers–Brillouin (WKB) approximation to Zener tunneling[8] has been widely used for its simplicity and its readiness. It has been recently applied to InP, InAs, and InSb nanowires with a direct band gap.[9,10] However, its application to materials with an indirect band gap such as Si or Ge, where phonon-assisted tunneling (PAT) is present, remains questionable. PAT has already been modeled in bulk[11] and 1D structures[12] using different approximations but not in nanowires.

We have developed a three-dimensional, atomistic, full-band quantum transport solver based on the nearest-neighbor tight-binding model and on the nonequilibrium Green's function (NEGF) formalism that models coherent transport in large cross section devices[3] and includes electron-phonon scattering in smaller devices.[13,14] It can self-consistently simulate direct and PAT in realistically extended nanowire TFETs and compute their complex bandstructure. The latter is used as an input parameter to WKB-based tunneling calculations. Then, the WKB results are compared to the full-band simulations to check their validity.

After a short description of the simulation approach in Sec. II, the transfer characteristics of InAs, Si, and Ge nanowire TFETs based on three methods are computed in Sec. III: (1) the WKB approximation (few seconds on a single CPU), (2) a quantum transport solver with direct tunneling only (few hours on a small cluster), and (3) with direct and PAT (several hours on a supercomputer). Since the computational burden drastically increases with the model accuracy, it is essential to determine the application range of each model. We will show that (i) the WKB approximation relies on the presence of a single dominant imaginary band between the VB and CB with "least action for tunneling"[15] as in InAs nanowires and fails in the other cases, (ii) phonon-*absorption* characterizes the TFET OFF-currents,[16] (iii) the tunneling current in Si and Ge nanowires with multiple crossing and mixing of imaginary bands can in general only be resolved with electron-phonon scattering, and (iv) direct tunneling can be sufficient in Ge under certain bias conditions. The paper is concluded in Sec. IV.

## II. SIMULATION APPROACH

The nearest-neighbor $sp^3d^5s^*$ tight-binding method has been chosen as bandstructure model for its ability to accurately reproduce the CB and the VB of Si,[17] Ge,[17] and InAs.[18] The accuracy of these models has been tested through quantitative agreement of simulations with experimental data in $Si/SiO_2/Si$ junctions,[19,20] strained InGaAs quantum dots,[21] single impurity in Si FinFETs,[22] and strained Si quantum wells on SiGe.[23] To reduce the computational burden, spin-orbit coupling (SO) is neglected. Consequently,

[a]Electronic mail: mluisier@purdue.edu.

 

the semiconductor band gaps and the effective masses are artificially altered, especially in the Ge and InAs nanowires. However, it has been verified that for the structures considered in this work, close to the CB and VB extrema, the band gap and the effective masses change by less than 5% and the basic structure of the complex band gap dispersion does not vary.

As an alternative, the nearest-neighbor $sp^3s^*$ tight-binding method with SO coupling could be used. The computational burden is the same as for $sp^3d^5s^*$ without SO, the InAs bandstructure and the VBs of Si and Ge are accurately reproduced, but the effective masses and gaps of Si and Ge along the $X$-valley are not accurate enough to correctly model band-to-band tunneling. The error is larger than the 5% observed when SO is neglected in the $sp^3d^5s^*$ model. Since it is more convenient to apply the same bandstructure model to all the device types, the $sp^3d^5s^*$ variant has been used in all cases.

Quantum transport and electron-phonon scattering are solved in the NEGF formalism in the self-consistent Born approximation.[13,14] The scattering self-energies are approximated to be diagonal in space

$$\Sigma_{nn}^{\gtrless,e-ph}(E) = \sum_{l} \sum_{\lambda,q} \mathbf{M}_{nl}^{\lambda}(q) \cdot \{N^{\lambda}(q)\mathbf{G}_{ll}^{\gtrless}[E \pm \hbar\omega_{\lambda}(q)] + [N^{\lambda}(q)+1]\mathbf{G}_{ll}^{\gtrless}[E \mp \hbar\omega_{\lambda}(q)]\} \cdot \mathbf{M}_{ln}^{\lambda *}(q). \quad (1)$$

The phonon bath, characterized by a mode $\lambda$, a wave vector $q$, and a frequency $\omega_{\lambda}(q)$, is assumed in equilibrium and is distributed according to the Bose statistics, $N^{\lambda}(q)$. The indices $\lambda$ and $q$ run over the complete dispersion of the confined phonons calculated according to Ref. 24. The matrix elements $\mathbf{M}_{nl}^{\lambda}(q)$ connect two nearest-neighbor atoms located at $\mathbf{R}_n$ and $\mathbf{R}_l$ and are defined as in Ref. 14. They account for the relative angle and distance dependence between one atom and its neighbors. The retarded $\mathbf{G}^R$, lesser $\mathbf{G}^<$, and greater $\mathbf{G}^>$ Green's functions are solved at each energy $E$ using a recursive algorithm.[25,26]

The band-to-band tunneling transmission in the WKB approximation is calculated as

$$T(E) = \exp\left[-2\int_{x_S(E)}^{x_D(E)} \mathrm{d}x\kappa(x)\right]. \quad (2)$$

The integration boundaries on the source side $x_S(E)$ and on the drain side $x_D(E)$ are determined from the CB and VB profiles extracted from the quantum transport simulations without electron-phonon scattering. Using the same electrostatic potential makes the comparison between the WKB and the quantum transport results independent from external factors. The decay rate $\hat{\kappa}(\mathcal{E})$ is computed in the tight-binding method as function of the energy $\mathcal{E}$.[13] Then, at each position $x$ between $x_S$ and $x_D$, the quantity $E-E_{VB}(x)$ is evaluated, where $E_{VB}(x)$ is the mean position-dependent VB edge of the device. Finally, $\kappa(x)$ is defined as $\hat{\kappa}[E-E_{VB}(x)]$, assuming that $\hat{\kappa}(0)$ represents the top of the VB.

One condition of application for the WKB approximation is that there is only one dominant imaginary band connecting the VB and CB, free from close interactions with other bands. Otherwise, it is not possible to unambiguously define a path with "least action for tunneling."[15] For example, when two imaginary bands "A" and "B" cross, an electron in band A cannot freely move into band B, except if the two bands have the same real part and the same symmetry properties (selection rules). If there are two close bands A and B, it is not clear whether $\hat{\kappa}_A$ or $\hat{\kappa}_B$ should be used in Eq. (2). Around a crossing point, a mixture of all the crossing imaginary bands is necessary, which goes much beyond the standard WKB approximation and will not be treated here.

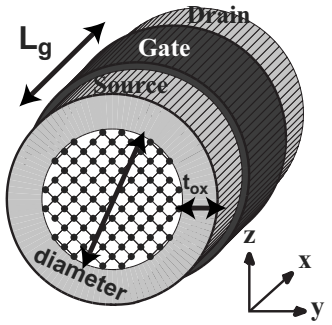


FIG. 1. Si, Ge, and InAs nanowire structure. The gate length $L_g$ measures 15 nm, the total nanowire length is 40 nm. The transport direction $x$ is aligned with the ⟨100⟩ crystal axis.

## III. RESULTS

We consider InAs, Si, and Ge $p$-$i$-$n$ gate-all-around nanowire TFETs as depicted in Fig. 1. The devices have a total length of 40 nm, composed of a $p^+$ source (12.5 nm), an intrinsic channel (15 nm), and a $n^+$ drain (12.5 nm) contact. The acceptor (donor) concentration in the source (drain) extension amounts to 2e20 $cm^{-3}$(1e20 $cm^{-3}$) for Si and Ge and 5e19 $cm^{-3}$(5e19 $cm^{-3}$) for InAs. The doping concentration is larger in the source than in the drain to create large electric fields at the source-channel interface and increase the tunneling probability. As a starting point, the nanowire diameter $d$ measures 3 nm for Si, 3.12 nm for Ge, and 3.35 nm for InAs so that the total number of atoms $N_A=14,089$ remains constant. All the nanowires are surrounded by a 1 nm-thick dielectric layer ($\epsilon_R=3.9$ for the Si and Ge structures and $\epsilon_R=9$ for the InAs transistor). The transport direction $x$ is aligned with the ⟨100⟩ crystal axis. The simulations are performed at room temperature. The small diameters and the resulting large band gaps of the nanowires do not allow for high performance TFETs but still represent good test cases for the different simulation approaches investigated in this work.

### A. InAs nanowire TFET

We start with the InAs nanowire TFET. The real and imaginary bands of an InAs nanowire with $d=3.35$ nm and $E_g=1.175$ eV are depicted in Fig. 2(a). Note that for clarity only few bands are represented. The imaginary dispersion (left part of the plot) is characterized by a single band (gray) that connects the lowest conduction subband to the highest valence subband and does not interact with any other imaginary band. This "isolated," nondegenerate, and imaginary

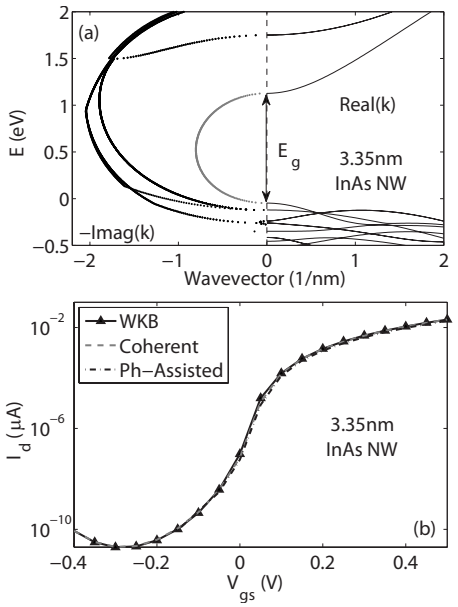


FIG. 2. (a) Imaginary (left part) and real (right part) band dispersion of an InAs nanowire with $d=3.35$ nm. (b) Transfer characteristics $I_d-V_{gs}$ at $V_{ds}=0.5$ V of an InAs nanowire TFET with $d=3.35$ nm calculated in the WKB approximation (solid line with triangles), including coherent tunneling only (dashed gray line), and with coherent and PAT (dashed-dotted line).

band is used in Eq. (2) to extract $\kappa(x)$ and to calculate the transfer characteristics of an InAs nanowire TFET with $d=3.35$ nm at $V_{ds}=0.5$ V.

The resulting current-voltage response is shown in Fig. 2(b) and compared to quantum transport simulations with and without PAT. All three models agree well, suggesting that (i) the WKB approximation, as implemented in Eq. (2), works well for TFETs based on a direct band gap material with a single dominant imaginary band connecting the VB and CB and assuming that a good estimate for the CB and VB profiles can be obtained and (ii) PAT is not important in InAs nanowire TFETs with a 15 nm gate length where source-to-drain tunneling leakage dominates the transistor OFF-state.[3]

The spectral ON-currents of the InAs nanowire TFET calculated in the WKB approximation and using the quantum transport approach of Sec. II with and without PAT are shown in Fig. 3. First, it can be observed that the spectral current simulated in the WKB approximation does not exhibit quantum resonances as the more advanced models do but it follows the same mean contour. Second, the spectral current with PAT is lower than the coherent current by about 10%. This is due to the fact that electron-phonon scattering can change the direction of propagation of VB electrons moving from the source to the channel. This effect is known as backscattering, it reduces the current magnitude and it has been well understood in conventional MOSFETs.[27]

It has been further verified that the WKB approximation still holds for InAs nanowire TFETs with larger diameters where the conduction subbands are closer in energy. A single dominant tunneling path can still be identified and used in the WKB approximation.

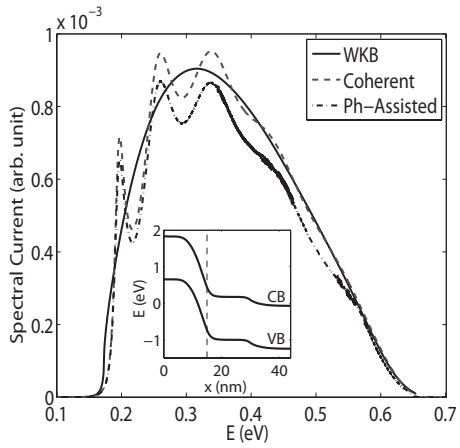


FIG. 3. Spectral current of an InAs nanowire TFET with $d=3.35$ nm at $V_{ds}=V_{gs}=0.5$ V extracted at the source-channel interface. The results obtained in the WKB approximation (solid line), with coherent tunneling only (dashed gray line), and with coherent and PAT (dashed-dotted line) are compared. The inset shows the band diagram and the line along which the spectral currents are extracted.

### B. Si nanowire TFET

Figure 4(a) shows the band gap dispersion of a Si nanowire with $d=3$ nm and $E_g=1.619$ eV. As for the InAs nanowire, not all the imaginary bands are plotted for clarity. Not all the band gap states are purely imaginary, some of them also have a real part when they originate from a band minimum or maximum away from the Γ point. This is an important characteristics since an electron cannot freely move from one imaginary band to the other if their momentum (real part of the band gap wave vector) are different. Such a transfer requires the absorption or emission of a phonon to ensure

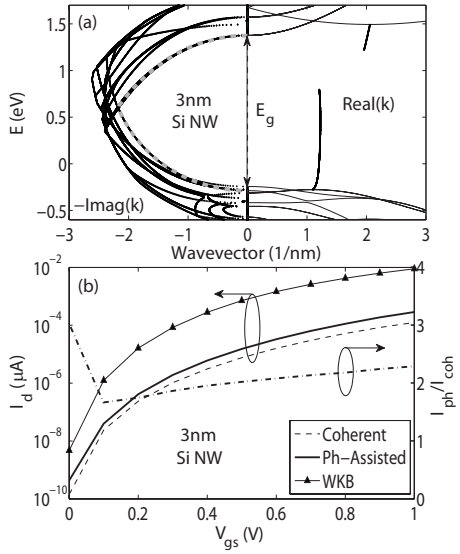


FIG. 4. (a) Imaginary (left part) and real (right part) band dispersion of a Si nanowire with $d=3$ nm. The real part of the band gap dispersion is also given. For clarity, not all the bands are shown. The dashed gray line follows the band used to calculate the WKB transmission according to Eq. (2). (b) Transfer characteristics $I_d-V_{gs}$ at $V_{ds}=1.0$ V (left axis) with PAT ($I_{ph}$, solid line) with coherent tunneling only ($I_{coh}$, dashed line), and in the WKB approximation ($I_{WKB}$, line with triangles) and ratio between $I_{ph}$ and $I_{coh}$ (dashed-dotted line, right axis) for a Si nanowire tunneling transistor with $d=3$ nm.

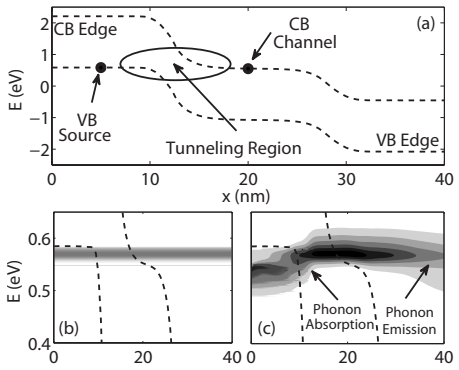


FIG. 5. (a) Band diagram of the Si TFET with $d=3$ nm at $V_{gs}=0$ V and $V_{ds}=1$ V (OFF-state). (b) Energy- and position-resolved current distribution in the coherent tunneling limit corresponding to the subplot (a). (c) Same as (b) but in the presence of PAT. The same color scale is used in the subplots (b) and (c).

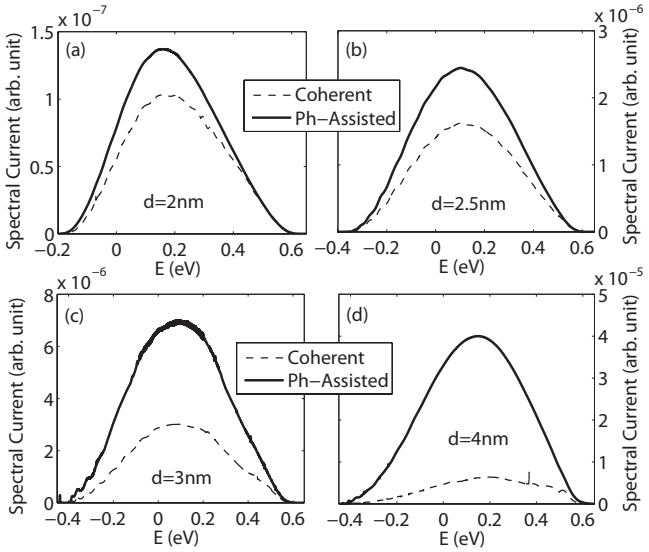


FIG. 6. Spectral currents at $V_{ds}=V_{gs}=1.0$ V extracted at the source-channel interface of Si nanowire TFETs with (a) $d=2$ nm, (b) $d=2.5$ nm, (c) $d=3$ nm, and (d) $d=4$ nm. The dashed curves refer to coherent tunneling only, the solid curves to coherent and PAT.

momentum conservation. Another relevant feature of the Si band gap dispersion is the presence of many tightly coupled imaginary bands connecting the top of the VB to the bottom of the CB. Especially, four complex bands originate from the lowest conduction subbands at Γ, one of them is directly connected to the third highest valence subband, and the three others are connected to low energy valence subbands out of which two are degenerate. It is therefore not possible to isolate one single path between the top of the VB and the bottom of the CB as for the InAs nanowire and as required by the WKB approximation.

The transfer characteristics of a Si nanowire TFET with $d=3$ nm is given in Fig. 4(b). It is simulated at $V_{ds}=1.0$ V using the quantum transport model described in Sec. II with (solid line) and without (dashed line) PAT and in the WKB approximation (line with triangles). The right axis of the figure indicates the ratio between the current with ($I_{ph}$) and without ($I_{coh}$) PAT. Neglecting PAT reduces the tunneling current by a factor 2, except at low $V_{gs}$, close to the transistor OFF-state, where the reduction factor exceeds 3.

As mentioned above, the absence of a dominant imaginary band between the CB and the VB does not allow to apply the WKB approximation and compare it to the quantum transport simulations. However, to highlight this problem, the imaginary band with the least action for tunneling, i.e., with the smallest $\kappa$, is used in Eq. (2) to simulate the Si device. The WKB approximation overestimates the device current by about two orders of magnitude, as illustrated in Fig. 4. This means that most of the states cannot use the selected imaginary band to tunnel from the VB to the CB, even in the presence of electron-phonon scattering and are spread over several imaginary bands. Consequently, the WKB approximation fails for Si nanowire TFETs.

The large ratio between the quantum transport currents with and without PAT close to the transistor OFF-state is explained in Fig. 5. When the minimum of the CB in the channel is only slightly below the maximum of the VB in the source contact, electrons see a small tunneling window. With direct tunneling only, VB electrons situated below the CB edge in the channel cannot reach the drain contact. However, the absorption of a phonon allows these electrons to reach states situated above the channel CB edge and to find their way to the other side of the device. This phenomenon enhances the OFF-current and has already been characterized in carbon nanotube TFETs.[16]

Apart from the region close to the transistor OFF-state, PAT enhances the current of the Si nanowire TFET by a factor of ≈2. In effect, electron-phonon scattering can bridge imaginary bands separated by an energy smaller than the maximum phonon energy and can compensate the momentum difference between two imaginary bands, if one of them also has a real part. This opens more channels from the VB to the CB, increasing the tunneling current. An electron that starts from a VB that would normally be connected to a high energy conduction subband with a high decaying rate can reach the minimum of the CB if it is transferred to a more favorable band by the absorption or emission of

Figure 6 shows that the inclusion of PAT becomes more important when the cross section of the Si nanowire TFET increases. The spectral ON-currents of devices with a diameter $d=2$, 2.5, 3, and 4 nm are reported for the cases with (solid lines) and without (dashed lines) PAT. The comparison is restricted to the ON-current due to the heavy computational resources required by the simulations of devices with a diameter larger than 3 nm. At a diameter $d=4$ nm, the TFET ON-current with direct tunneling only is 8 times smaller than the ON-current with PAT ($I_{ON,ph}=1.65$ nA, $I_{ON,coh}=0.196$ nA), while it is 1.29 times smaller for $d=2$ nm ($I_{ON,ph}=4.28$ pA, $I_{ON,coh}=3.32$ pA), 1.48 times for $d=2.5$ nm ($I_{ON,ph}=93.4$ pA, $I_{ON,coh}=63.1$ pA), and 2.3 times for $d=3$ nm ($I_{ON,ph}=0.289$ nA, $I_{ON,coh}=0.125$ nA). This indicates that PAT could eventually be neglected in very narrow devices, where the tunneling current is small anyway but when the TFET size increases and the device properties become more bulklike, PAT must be included to obtain the correct transistor characteristics.

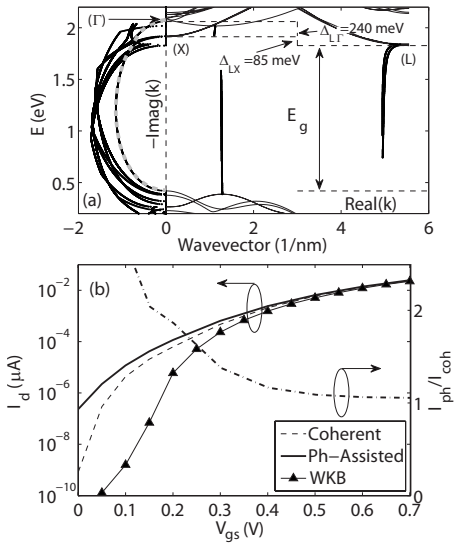


FIG. 7. (a) Imaginary (left part) and real (right part) band dispersion of a Ge nanowire with $d=3.12$ nm. The real part of the band gap dispersion is also given. For clarity, not all the bands are shown. The dashed gray line represents the least action for tunneling path. (b) Transfer characteristics $I_d-V_{gs}$ at $V_{ds}=0.7$ V (left axis) with PAT ($I_{ph}$, solid line), with coherent tunneling only ($I_{coh}$, dashed line), and in the WKB approximation ($I_{WKB}$, line with triangles) and ratio between $I_{ph}$ and $I_{coh}$ (dashed-dotted line, right axis) for a Ge nanowire TFET with $d=3.12$ nm.

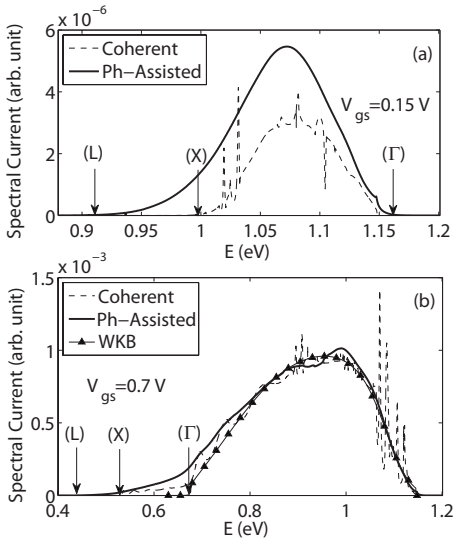


FIG. 8. (a) Spectral current of a Ge nanowire TFET with $d=3.12$ nm at $V_{ds}=0.7$ V and $V_{gs}=0.15$ V extracted at the source-channel interface. The dashed line refers to coherent tunneling only, the solid line to PAT. The position of the bands labeled ($L$), ($X$), and ($\Gamma$) in Fig. 7 is indicated. (b) Same as (a) but at $V_{gs}=0.7$ V. The results obtained in the WKB approximation (solid line with triangles) are also shown.

### C. Ge nanowire TFET

As a last example, a Ge nanowire TFET with $d=3.12$ nm and $E_g=1.409$ eV is considered. Its band gap dispersion is reproduced in Fig. 7(a). It only contains the most relevant imaginary bands, as well as the real part of certain bands. The eight bulk CB valleys of Ge at $L$ are projected to $k=\pi/a_0$ (four bands) and $k=-\pi/a_0$ (four bands), where $a_0$ is the lattice constant of Ge, and labeled ($L$) in Fig. 7(a). Four of the six bulk CB valleys along $X$ are projected to $\Gamma$ and labeled ($X$). The energy separation $\Delta_{LX}$ between the CB originating from $L$ and from $X$ amounts to 85 meV. In bulk Ge, the CB minimum at $\Gamma$ is situated only 140 meV above the $L$ valley minimum. In a nanowire with $d=3.12$ nm, the energy difference between the lowest conduction subband originating from the bulk $\Gamma$ valley and labeled ($\Gamma$) in Fig. 7(a) and the bands projected from the bulk $L$ valleys and labeled ($L$) increases to $\Delta_{L\Gamma}=240$ meV.

There is no imaginary band that directly connects the lowest conduction subbands ($L$) to the highest valence subbands. There is one imaginary band that apparently connects the conduction subbands labeled ($X$) to the top of the VB with a maximum decay rate $\kappa$ of 1.19 nm$^{-1}$. This band is nondegenerate, it does not have any real part contrary to the group of bands labeled ($L$), and it strongly interacts with other imaginary bands close to the CB minimum, obscuring the fact that it effectively originates from the ($\Gamma$) state and not ($X$), as demonstrated later. It is chosen as least action for tunneling path and represented by the dashed gray line in Fig. 7(a).

The transfer characteristics $I_d-V_{gs}$ at $V_{ds}=0.7$ V with (solid line) and without (dashed line) PAT of the Ge nanowire TFET is given in Fig. 7(b) as well as the ratio between $I_{ph}$ and $I_{coh}$ on the right axis. The transfer characteristics calculated in the WKB approximation with the most favorable imaginary band [dashed gray line in Fig. 7(a)] is also shown in Fig. 7(b). At low $V_{gs}$, the WKB approximation underestimates the tunneling current by several orders of magnitude but it improves as $V_{gs}$ increases to finally match the more advanced models close to the ON-current region.

In the quantum transport simulations, the neglection of PAT is more important at low $V_{gs}$ than at high $V_{gs}$ for the Ge nanowire TFET. Close to the transistor OFF-state, phonon absorption enhances the tunneling current as in Fig. 5. Then, when $V_{gs}$ increases, the $I_{ph}/I_{coh}$ ratio decreases to $\approx 1$, suggesting that direct tunneling is sufficient to capture the ON-current region. This can be understood from the imaginary and real bands of the Ge nanowire in Fig. 7(a) and by considering the spectral currents of the Ge nanowire TFET at different $V_{gs}$ shown in Fig. 8.

The tunneling window of the Ge nanowire extends from the minimum of the CB in the channel, the ($L$) bands, whose position can be shifted by the gate contact, up to the maximum of the VB in the source fixed at $E_{VB}=1.15$ eV. At $V_{gs}=0.15$ V, the ($L$) bands in the channel are situated at $E_L=0.92$ eV, the ($X$) bands at $E_X=1.05$ eV, and the first ($\Gamma$) band at $E_\Gamma=1.16$ eV. Hence, the apparent tunneling window for the ($L$) bands is about 230 meV, 145 meV for the ($X$) bands, and 0 meV for the ($\Gamma$) band. However, since there is no imaginary band connecting the top of the VB to the ($L$) bands, no tunneling is possible for energies lower than $E_X$ when electron-phonon scattering is neglected. Hence, no coherent current flows for energies comprised between $E_L$ and $E_X$ as illustrated in Fig. 8(a). Then, for energies larger than $E_X$, the ($X$) conduction subbands become available in the nanowire channel and both direct and PAT are present. The absorption or emission of a phonon still improves the tunneling current, suggesting that the imaginary bands that directly

connect the VB and the CB labeled ($X$) interact with other bands whose decaying rate is smaller than its own, like the dashed gray line in Fig. 7(a).

As $V_{gs}$ increases, the band minimum $E_L$, $E_X$, and $E_\Gamma$ are pushed down to become $E_L$=0.43 eV, $E_X$=0.515 eV, and $E_\Gamma$=0.67 eV at $V_{gs}$=0.7 V, leading to apparent tunneling windows of 0.72 eV, 0.635 eV, and 0.48 eV, respectively. At this gate voltage, the currents calculated with and without PAT as well as in the WKB approximation are about the same. This is illustrated in Fig. 8(b), where the spectral current of the Ge nanowire TFET at $V_{gs}$=0.7 V is given. The main current contribution comes from energies larger than $E_\Gamma$, i. e., when the CB labeled ($\Gamma$) in Fig. 7(a) becomes available in the channel. Since this CB originates from a bulk $\Gamma$-state, no PAT is required to move electrons from the VB to it, exactly as for the InAs nanowire in Sec. III A. Between $E_L$ and $E_X$, only PAT is possible, while between $E_X$ and $E_\Gamma$, electron-phonon interaction enhances the tunneling current which remains much smaller than for energies larger than $E_\Gamma$.

The WKB approximation becomes accurate at large $V_{gs}$ because the device current is dominated by direct tunneling occurring between the top of the VB and the CB labeled ($\Gamma$), which are connected by the imaginary band that has been chosen as the path for least action for tunneling. However, the WKB cannot correctly capture the characteristics of the Ge nanowire TFET when the current is dominated by direct or PAT from the top of the VB to the ($L$) and ($X$) CB as for low $V_{gs}$. In other words, the WKB approximation starts working when $E_\Gamma$ is pushed well below the maximum of the source VB.

The ON-currents of Ge nanowire TFETs with smaller and larger diameters have also been simulated with and without PAT. At a diameter $d$=2 nm, the $I_{ph}/I_{coh}$ ratio is slightly smaller than 1 ($I_{ON,ph}$=0.4 nA, $I_{ON,coh}$=0.45 nA). At $d$=4.1 nm, the ON-currents with and without PAT are almost identical ($I_{ON,ph}$=42.3 nA, $I_{ON,coh}$=41.7 nA). Due to numerical and computational restrictions, it is not possible to simulate devices with a diameter larger than 4.1 nm, but it seems that coherent quantum transport simulations of Ge nanowire TFETs are able to deliver a very good estimate of the device ON-current, which is dominated by electrons tunneling from the top of the VB to the lowest CB state originating from the bulk $\Gamma$ valley.

## IV. CONCLUSION

We have simulated InAs, Si, and Ge nanowire TFETs in the WKB approximation and with an atomistic and full-band quantum transport solver. It has been demonstrated that the WKB approximation agrees well with the more complicated models for the InAs structure only but fails for the Si and Ge devices, where quantum effects and PAT dominate. However, the ON-current of the Ge nanowire device, due to its particular CB configuration, is almost insensitive to PAT and it can be accurately predicted by a coherent simulation.

## ACKNOWLEDGMENTS

The authors would like to thank Timothy Boykin for helpful discussions. This work was partially supported by NSF under Grant No. EEC-0228390 that funds the Network for Computational Nanotechnology, by NSF PetaApps under Grant No. OCI-0749140, by the Nanoelectronics Research Initiative through the Midwest Institute for Nanoelectronics Discovery, and by NSF through TeraGrid resources provided by the National Institute for Computational Sciences (NICS). This research also used resources of the National Center for Computational Sciences at Oak Ridge National Laboratory, which is supported by the Office of Science of the U.S. Department of Energy under Contract No. DE-AC05-00OR22725.

[1] J. Appenzeller, Y.-M. Lin, J. Knoch, and Ph. Avouris, Phys. Rev. Lett. **93**, 196805 (2004).
[2] W. Y. Choi, B.-G. Park, J. D. Lee, and T.-J. King Liu, IEEE Electron Device Lett. **28**, 743 (2007).
[3] M. Luisier and G. Klimeck, IEEE Electron Device Lett. **30**, 602 (2009).
[4] J. Appenzeller, J. Knoch, M. T. Björk, H. Riel, and W. Riess, IEEE Trans. Electron Devices **55**, 2827 (2008).
[5] M. M. Rieger and P. Vogl, Phys. Rev. B **48**, 14276 (1993).
[6] M. V. Fischetti and S. E. Laux, J. Appl. Phys. **80**, 2234 (1996).
[7] A. Bowonder, P. Patel, K. Jeon, J. Oh, P. Majhi, H.-H. Tseng, and C. Hu, International Workshop on Junction Technology (IWJT), 2008 , pp. 93–96.
[8] S. M. Sze, *Physics of Semiconductor Devices*, 2nd ed. (Wiley, New York, 1981).
[9] M. A. Khayer and R. K. Lake, Appl. Phys. Lett. **95**, 073504 (2009).
[10] M. A. Khayer and R. K. Lake, IEEE Electron Device Lett. **30**, 1257 (2009).
[11] A. Schenk, Solid-State Electron. **36**, 19 (1993).
[12] C. Rivas, R. Lake, G. Klimeck, W. Frensley, M. V. Fischetti, P. E. Thompson, S. L. Rommel, and P. R. Berger, Appl. Phys. Lett. **78**, 814 (2001).
[13] M. Luisier, G. Klimeck, A. Schenk, and W. Fichtner, Phys. Rev. B **74**, 205323 (2006).
[14] M. Luisier and G. Klimeck, Phys. Rev. B **80**, 155430 (2009).
[15] S. E. Laux, J. Comput. Electron. (in press).
[16] S. O. Koswatta, M. S. Lundstrom, and D. E. Nikonov, Appl. Phys. Lett. **92**, 043125 (2008).
[17] T. B. Boykin, G. Klimeck, and F. Oyafuso, Phys. Rev. B **69**, 115201 (2004).
[18] T. B. Boykin, G. Klimeck, R. Chris Bowen, and F. Oyafuso, Phys. Rev. B **66**, 125207 (2002).
[19] M. Städele, B. R. Tuttle, and K. Hess, J. Appl. Phys. **89**, 348 (2001).
[20] F. Sacconi, A. di Carlo, P. Lugli, M. Städele, and J. M. Jancu, IEEE Trans. Electron Devices **51**, 741 (2004).
[21] M. Usman, H. Ryu, I. Woo, D. S. Ebert, and G. Klimeck, IEEE Trans. Nanotechnol. **8**, 330 (2009).
[22] G. P. Lansbergen, R. Rahman, C. J. Wellard, P. E. Rutten, J. Caro, N. Collaert, S. Biesemans, I. Woo, G. Klimeck, L. C. L. Hollenberg, and S. Rogge, Nat. Phys. **4**, 656 (2008).
[23] N. Kharche, M. Prada, T. B. Boykin, and G. Klimeck, Appl. Phys. Lett. **90**, 092109 (2007).
[24] Z. Sui and I. P. Herman, Phys. Rev. B **48**, 17938 (1993).
[25] A. Svizhenko, M. P. Anantram, T. R. Govindan, B. Biegel, and R. Venugopal, J. Appl. Phys. **91**, 2343 (2002).
[26] R. Lake, G. Klimeck, R. C. Bowen, and D. Jovanovic, J. Appl. Phys. **81**, 7845 (1997).
[27] M. S. Lundstrom, IEEE Electron Device Lett. **22**, 293 (2001).